ELSEVIER

Journal of Hazardous Materials 142 (2007) 550–554

Journal of Hazardous Materials

www.elsevier.com/locate/jhazmat

Short communication

A new high-nitrogen compound $[Mn(ATZ)(H_2O)_4]\cdot 2H_2O$: Synthesis and characterization

Bao-Juan Jiao [a], San-Ping Chen [a], Feng-Qi Zhao [a,b], Rong-Zu Hu [a,b], Sheng-Li Gao [a,*]

[a] *Department of Chemistry, Shaanxi Key Laboratory of Physico-Inorganic Chemistry, Northwest University, Xi'an 710069, China*

[b] *Xi'an Modern Chemistry Research Institute, Xi'an, Shaanxi 710065, China*

Received 17 January 2006; received in revised form 27 July 2006; accepted 28 July 2006

Available online 3 August 2006

Abstract

A new high-nitrogen compound $[Mn(ATZ)(H_2O)_4]\cdot 2H_2O$ (ATZ = 5,5-azotetrazolate) was synthesized. Crystal structure and elemental, IR and thermal analyses were investigated in the present work. It crystallized in triclinic space group *P*-1 with lattice parameters $a = 6.304(2)$ Å, $b = 7.004(2)$ Å, $c = 7.921(3)$ Å, $\alpha = 76.114(5)^\circ$, $\beta = 74.023(5)^\circ$, $\gamma = 69.254(4)^\circ$. TG-DTG and DSC measurements are employed to postulate the thermal decomposition mechanism. The thermal decomposition kinetics of the main exothermic reaction was investigated by non-isothermal method and obtained its enthalpy of decomposition and the probable kinetic mechanism. An attempt was made to incorporate the relation between thermal stability and the structure.

Keywords: ATZ^{2-}; Crystal structure; Single crystal; Thermal analysis

1. Introduction

Modern high-energy density materials (HEDM) derive most of their energy either (i) from oxidation of the carbon backbone, as with traditional energetic materials [1–2] or (ii) from their very high positive heat of formation. Nitrogen-rich compounds are new members of the second family and they are environmentally acceptable [3]. They rely on their highly efficient gas production and also on their high heat of formation for energy release, since elemental nitrogen, which has a zero heat of formation, is the major product of decomposition. After Thiele prepared metallic salts of azotetrazole and claimed these for use in initiators, salts of ATZ^{2-} have been extensively investigated [4–6] and have often been considered for practical use as a class of energetic materials.

Kinetic and thermodynamic characterization of chemical reactions is a crucial task in the context of thermal process safety as well as process development [7]. In brief, using modern thermal analysis techniques such as TG-DTG and DSC, the thermal behavior of materials may be determined in a short time using milligram quantities. For the purpose of scale-up as well as kinetic and thermodynamic analysis of a desired decomposition reaction, non-isothermal reaction measurements are mostly preferred.

In this paper, we report on the synthesis and characterization of $[Mn(ATZ)(H_2O)_4]\cdot 2H_2O$, which is a new member of the high-nitrogen compound. The X-ray structure analysis reveals the bonding mode of ATZ^{2-} with Mn^{2+}. Thermal analyses of TG-DTG and DSC of the investigated compound are discussed. Moreover, the transformation of the microcosmic structure was elaborated in the thermal decomposition process of the title compound. Based on thermodynamic data obtained by non-isothermal methods, the present work can project the probable application of the compound in the area of high-energy materials.

2. Experimental

2.1. Materials

All reagents used for the syntheses were purchased from commercial sources and used without further purification.

* Corresponding author.
E-mail address: gaoshli@nwu.edu.cn (S.-L. Gao).

0304-3894/$ – see front matter © 2006 Elsevier B.V. All rights reserved.
doi:10.1016/j.jhazmat.2006.07.066

2.2. Synthesis

Synthesis of $Na_2ATZ{\cdot}5H_2O$: the oxidation of 5-aminotetrazole with potassium permanganate in basic aqueous solution yields disodium 5,5′-azotetrazolate pentahydrate [8].

Synthesis of $[Mn(ATZ)(H_2O)_4]{\cdot}2H_2O$: yellow block-like crystal for X-ray diffraction analysis was obtained from the mixture of $MnCl_2{\cdot}H_2O$ (0.188 g, 1 mmol), $Na_2ATZ{\cdot}5H_2O$ (0.304 g, 1 mmol) and distilled H_2O (10 mL), which was allowed to evaporate at room temperature for 1 week, the compound was filtered and air dried. Yield: 76%. Anal. Calcd. $MnC_2N_{10}O_6H_{12}$ weight (%): C, 7.34; H, 3.70; N, 42.82. Found: C, 7.14; H, 3.80; N, 42.52.

2.3. Analytical methods and equipments

Mn^{2+} was determined with EDTA by complexometric titration, Cl^- was checked with $AgNO_3$ solution and Na^+ was identified with uranium (VI) zinc acetate ($Zn(UO_2)_3(Ac)_8$) solution. C, H and N analyses were carried out using an instrument of Vario EL III CHNOS of Germany. Infrared (IR) spectra drawn at regular intervals were recorded on a Bruker FTIR instrument as KBr pellets. The TG-DTG analysis was conducted on a P.E. 2100 Company thermal analyzer in a 100 mL/min N_2 (99.999%) atmosphere from room temperature to 800 °C. DSC experiment was performed using the thermal analyzer of Shanghai Balance Instrument factory under a 100 mL/min nitrogen from ambient temperature to 500 °C. Before starting a test, a sample was flushed with the nitrogen gas for 10 min to eliminate residual air presented in the system. The sample was then heated at a projected constant rate 10.0 °C/min with the mass of 0.5 mg. XRD patterns were measured on a Rigaku D/max-IIIA X-ray diffractometer with graphite monochromatized Cu Kα (λ = 1.54056 Å).

Table 1
Crystal data and structure refinement data for title compound

Empirical formula	$C_2H_{12}MnN_{10}O_6$
Formula weight	327.16
Crystal system	Triclinic
Temperature (K)	273(2)
Space group	*P*-1
a (Å)	6.3045(2)
b (Å)	7.004(2)
c (Å)	7.921(3)
α (°)	76.114(5)
β (°)	74.023(5)
γ (°)	69.254(4)
Z	1
D_c (mg m^{-3})	1.750
F (0 0 0)	167
Theta range for data collection (°)	3.15–25.54
Absorption coefficient (mm^{-1})	1.108
Limiting indices	$-7 \le h \le 7$, $-8 \le k \le 8$, $-9 \le l \le 6$
Goodness-of-fit on F^2	1.081
Reflections collected/unique	1664/1144 [*R*(int) = 0.0115]
Final *R* indices [$I > 2\sigma(I)$]	$R_1 = 0.0309$, w$R_2 = 0.0910$
R indices (all data)	$R_1 = 0.0338$, w$R_2 = 0.0921$
Largest difference peak and hole (e nm^{-3})	0.266 and −0.557

Table 2
Selected bond lengths (Å) and bond angles (°)

Mn(1)–O(1)	2.1439(19)
Mn(1)–O(2)	2.1718(19)
Mn(1)–N(1)	2.3081(19)
O(1)#1–Mn(1)–O(1)	180.0
O(1)#1–Mn(1)–O(2)#1	89.66(9)
O(1)–Mn(1)–O(2)#1	90.34(9)
O(1)–Mn(1)–O(2)	89.66(9)
O(2)#1–Mn(1)–O(2)	180.0
O(1)#1–Mn(1)–N(1)#1	91.16(7)
O(1)–Mn(1)–N(1)#1	88.84(7)
O(2)#1–Mn(1)–N(1)#1	89.49(7)
O(2)–Mn(1)–N(1)#1	90.51(7)
O(1)#1–Mn(1)–N(1)	88.84(7)
O(1)–Mn(1)–N(1)	91.16(7)
O(2)#1–Mn(1)–N(1)	90.51(7)
O(2)–Mn(1)–N(1)	89.49(7)
N(1)#1–Mn(1)–N(1)	180.0

Symmetry operations: #1: $-x+1$, $-y+1$, $-z+1$.

The accelerating voltage was set at 35 kV with 40 mA flux at a scanning rate of 0.05°/s in the 2*θ* range of 10–60°.

2.4. X-ray data collection and structure determination

The single crystal X-ray experiment was performed on a Bruker Smart Apex CCD diffractometer equipped with graphite monochromatized Mo Kα radiation (λ = 0.71073 Å) using ω and φ scan mode. The single-crystal structure of complex was solved by direct methods and refined with full-matrix least-squares refinements based on F^2 using SHELXS 97 and SHELXL 97 [9–10]. All non-H atoms were located using subsequent Fourier-difference methods. In all cases hydrogen atoms were placed in calculated positions and thereafter allowed to ride on their parent atoms. Other details of crystal data, data collection parameters and refinement statistics are given in Table 1. Selected bond distances and bond angles are given in Table 2.

3. Results and discussion

The two strong absorptions in the IR spectra of the compound at 1400 and 733 cm^{-1} exhibited the characteristic frequencies for asymmetrical CN_3 stretching mode and asymmetrical CN_2 one of tetrazole ring, respectively.

Single-crystal analysis shows the complex crystallizes in triclinic space group *P*-1 and exists as a one-dimensional infinite chain. As shown in Fig. 1, the coordination geometry around Mn(II) ion can be described a disordered octahedral arrangement with coordination number of 6, where O1, O2, O1A and O2A form the equatorial plane, and axial positions are occupied by N1 and N1A. Additionally, each ATZ^{2-} provides two terminal nitrogen atoms (N1 and N1A) acting as bridging ligand to connect two $[Mn(H_2O)_4]^{2+}$ to form an infinite zigzag chain. Furthermore, O1 atom from the one-dimensional infinite chain and the lattice water atom (O3) act as two hydrogen-bonding donors to interact with acceptors of O3, N4 and N3, N2 atoms from the adjacent chain, with 2.701(3) Å for O(1)–H(1A) . . . O(3); 2.850(3) Å for O(1)–H(1B) . . . N(4); 2.845(3) Å for O(3)–H(3A)

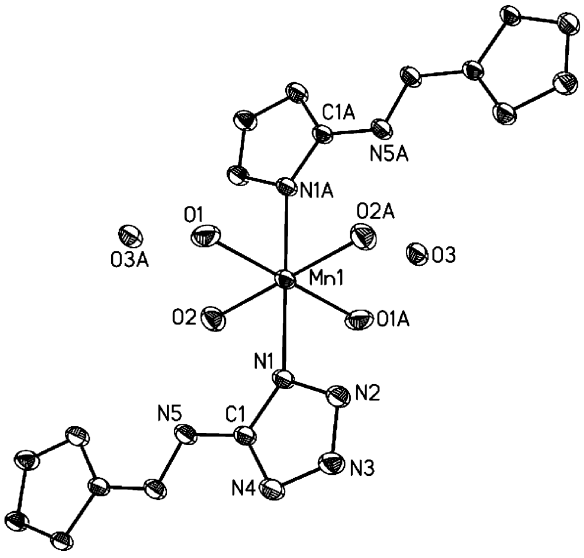

Fig. 1. View of coordination environment of the Mn(II) ion with the atom numberings scheme. Displacement ellipsoids are drawn at the 30% probability.

... N(3); 2.852(3) Å for O(3)–H(3B) ... N(2), resulting in a three-dimensional supramolecular network.

In order to evaluate the thermal stability of the synthesized compound, TG-DTG and DSC experiments were employed under N_2 atmosphere. As shown in Table 3 and Figs. 2 and 3, there is a good interpretive agreement of the postulated thermal decomposition processes and energy changes between TG-DTG and DSC results.

The weight loss corresponding to the crystal water molecular and the coordinated ones belong to the former two processes of decomposition, respectively. The fact shows clearly that the loss of water from compound occurs at different temperatures depending on the way that the water molecular is bound in the compound. The compound loses water bound with hydrogen bonds faster than that with the coordination bonds. As for the

Table 3
The postulated decomposition mechanism of the title compound

	T_0 (°C)	T_p (°C)	T_f (°C)	$\Delta_r H$ (J/g)	Residual mass (%)
I. Possible residual, $Mn(ATZ)(H_2O)_4$					
DSC	25.00	76.43	88.83	316.8 (en)	
TG-DTG	25.00	71.89	87.49	88.89 (F)	88.99 (C)
II. Possible residual, Mn(ATZ)					
DSC	88.83	115.38	133.44	435.4 (endo)	
TG-DTG	87.49	114.54	134.00	66.89 (F)	66.96 (C)
III. Possible residual, $(1/2)(Mn(ATZ)\cdot MnO_2)$					
DSC	133.44	166.01	288.08	578.3 (exo)	
TG-DTG	134.21	164.84	288.20	47.17 (F)	46.77 (C)
IV. Possible residual, MnO_2					
DSC	288.08	367.32	405.25	2371.0 (exo)	
TG-DTG	288.20	352.120	407.00	27.10 (F)	26.58 (C)
V. Possible residual, Mn_2O_3					
TG-DTG	407.00	755.6	780.00	23.94 (F)	24.13 (C)

Notes: endo, endothermic; exo, exothermic; F, experimental; C, calculated.

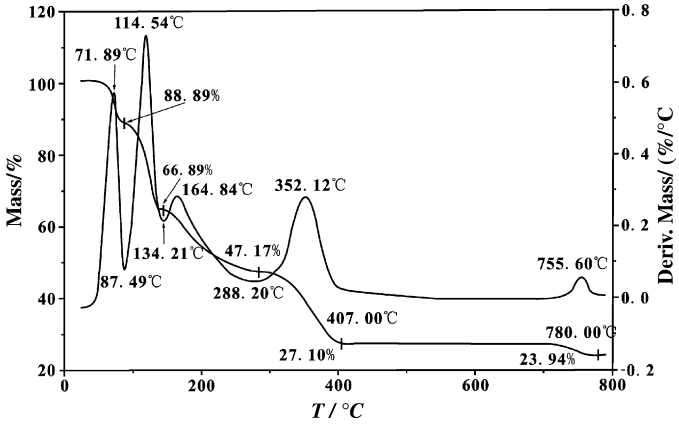

Fig. 2. TG-DTG curves of the title compound at 10 °C/min.

DSC experiment, the results support the two endothermic processes.

Accompanying with the loss of water, the exothermic decomposition follows immediately. This phenomenon gives some hints that it is not possible to dry the compound at higher temperature (lower than 130 °C at N_2 atmosphere). That is, the loss of water decreases the stability of the compound. After dehydration, the nitrogen content of the residual increases to 63.95 wt.%, implying the enhancement of energy. On the other hand, the transformation of crystal structure throws light on the instability of the dehydration product. The zigzag one-dimensional chain would be existed in the π–π stacking interactions among the ligands (centroid-plane distance = 0.3415 nm). Obviously, the π–π stacking interactions are not enough to stabilize the dehydration product at a higher temperature. The exothermic step in DSC curve indicates the collapses of the stacking of crystal structure and the following partial decomposition of the residual. XRD diffraction pattern of the decomposed products (Fig. 4) reveals that there is MnO_2 occurrence (JPCDS 82-2169).

After the first exothermic decomposition process, there is an obvious exothermic reaction faster than the former process with a reaction heat of 2371.0 J g^{-1}. The more heat and shorter reaction temperature intervals may be attributed to the produce

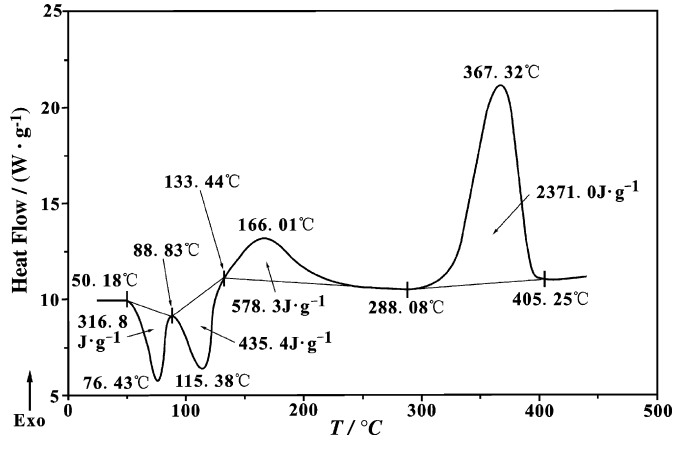

Fig. 3. DSC curve of the title compound at 10 °C/min.

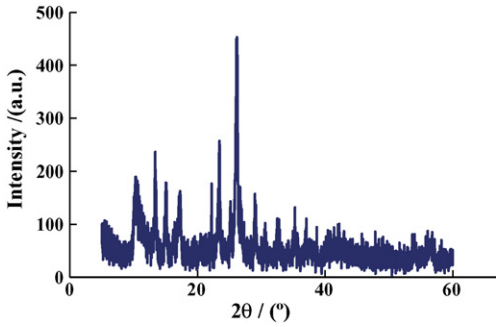

Fig. 4. XRD diffractional pattern of the products of the third decomposition process.

Table 4
The kinetic analysis methods

Method	Equations	
Ordinary-Integral	$\ln[G(\alpha)/T^2] = \ln[(AR/\beta E)(1-2RT/E)] - E/RT$	(1)
Uivenrsal-Integral	$\ln[G(\alpha)/(T-T^0)] = \ln A/\beta - E/RT$	(2)
Mac Callum-Tanner	$\lg[G(\alpha)] = \lg(AE/\beta R) - 0.4828E^{0.4357} - (0.449 + 0.217E)/0.001T$	(3)
Šatava-Šesták	$\lg G(\alpha) = \lg(AE/\beta R) - 2.315 - 0.4567E/RT$	(4)
Agrawal	$\ln[G(\alpha)/T^2] = \ln\{(AR/\beta E)[1-2RT/E]/[1-5(RT/E)^2]\} - E/RT$	(5)

of MnO_2. Seeing from the structure, the abruptly increasing of heat owes to the rupture of the skeleton.

The kinetics of exothermic reactions is important in assessing the potential of materials. In order to obtain the values of E_a and A of the fourth decomposition process from a single non-isothermal DSC curve, five integral equations are employed as listed in Table 4. Where α is the fractional decomposition, T the temperature (°C) at time t, R the gas constant, A the pre-exponential factor, E_a the apparent activation energy, β the hating rate, $G(\alpha)$ the integral mechanism functions, T_0 the initial point at which DSC curve deviates from the baseline, T_p the peak temperature of DSC curve, and dH/dt is the exothermic heat flow

Table 5
Data needed for kinetic calculation of the fourth decomposition process from DSC curve

T (°C)	a	dH/dt (mJ/s)	T (°C)	a	dH/dt (MJ/s)
349	21.06	8.7072	364	52.13	10.0512
350	22.74	8.8752	365	52.51	10.0656
351	24.39	9.0288	366	56.86	10.0896
352	26.37	9.1872	367	57.89	10.1136
353	28.33	9.3264	368	61.43	10.1328
354	30.38	9.4608	369	63.88	10.1280
355	32.19	9.5808	370	65.98	10.0992
356	32.97	9.6912	371	67.38	10.0512
357	36.46	9.7776	372	70.89	9.9792
358	38.61	9.8400	373	73.28	9.8880
359	40.81	9.8976	374	75.48	9.7728
360	43.09	9.9504	375	76.68	9.6336
361	45.44	9.9840	376	79.85	9.4848
362	47.7	10.0080	377	81.93	9.3072
363	49.9	10.0224	378	83.84	9.1056

$T_0 = 289$ °C, $T_p = 332$ °C, $H_0 = 1138.08$ mJ, $\beta = 10$ °C/min.

Table 6
Results of kinetic calculation for the fourth decomposition process

Method	E (kJ/mol)	lg[A] (s^{-1})	r	Q
Ordinary-Integral	147.64	11.6879	0.9892	0.0945
Uivenrsal-Integral	148.51	10.5448	0.9894	0.0402
Mac Callum-Tanner	150.7	11.9252	0.9906	0.0177
Šatava-Šesták	150.46	11.9398	0.9906	0.0177
Agrawal	147.64	11.3587	0.9892	0.0912
Mean	148.99	11.4913		

at time t. Forty-one types of kinetic model functions [11] and the original data tabulated in Table 5 are put into Eqs. (1) and (5) for calculation, respectively. The probable kinetic model function was selected by the better value of r, and Q. The values of E_a, A, linear correlation coefficient (r), and standard mean square deviation (Q) obtained by Eqs. (1) and (5) on the computer are listed in Table 6. The values of E_a are very close to each other. As a result, the Mampel Power principle ($n = 1$) of $f(\alpha) = 1$ controls the decomposition process.

4. Conclusions

Compound $[Mn(ATZ)(H_2O)_4]\cdot 2H_2O$ (ATZ = 5,5-azotetrazolate) was synthesized.

Crystal structure showed Mn(II) ion was coordinated with six atoms, forming a distorted octahedron configuration. The thermal stability of the compound from room temperature to 800 °C was performed and the structure was responsible for the postulated decomposition processes. The thermal decomposition kinetics of the main exothermic reaction was $f(\alpha) = 1$ and the apparent active energy was 148.99 kJ/mol.

Caution: While all hydrates of 5,5-azotetrazolate salts are insensitive to shock and friction, the anhydrous 5,5-azotetrazolate salts are very sensitive. Safety equipment such as leather gloves, face shields and earplugs are necessary.

Acknowledgements

We gratefully acknowledge the financial support from the National Natural Science Foundation of China (grant no. 20471047), Education Committee Foundation of Shaanxi Province (grant no. 05JK291), the Nature Science Foundation of Shaanxi Province (grant nos. FF05201 and FF05203) and the Science and Technology Foundation of the National Defense Key Laboratory of Propellant and Explosive Combustion of China (grant no. 51455010105QT3001).

Appendix A. Supplementary material

CCDC 295189 contains the supplementary crystallo-graphic data for this paper. These data can be obtained free of charge at http://www.ccdc.ac.uk/conts/retrieving.html or from the Cambridge Crystallographic Data Center (CCDC), 12 Union Road, Cambridge CB21EZ, UK. Fax: +44 1223 336033; e-mail: deposit@ccdc.cam.ac.uk.

References

[1] H. Feuer, A.T. Nielsen, NitroCompounds Recent Advances in Synthesis and Chemistry, VCH, New York, 1990.

[2] A.T. Nielsen, Nitrocarbons, Polycyclic Amine Chemistry, VCH, New York, 1995.

[3] (a) D.E. Chavez, M.A. Hiskey, R.D. Gilardi, 3,3′-Azobis(6-amino-1,2,4,5-tetrazine): a novel high-nitrogen energetic material, Angew. Chem. 112 (10) (2000) 1861–1863;
D.E. Chavez, M.A. Hiskey, R.D. Gilardi, 3,3′-Azobis(6-amino-1,2,4,5-tetrazine): a novel high-nitrogen energetic material, Angew. Chem., Int. Ed. 39 (2000) 1791;
(b) W. Fraenk, T. Habereder, A. Hammerl, T.M. Klapötke, B. Krumm, P. Mayer, H. Nöth, M. Warchhold, Highly energetic tetraazidoborate anion and boron triazide adducts, Inorg. Chem. 40 (2001) 1334–1340;
(c) A. Hammerl, G. Holl, M. Kaiser, T.M. Klapötke, H. Piotrowski, Synthesis and characterization of hydrazinium azide hydrazinate, Propell. Explos. Pyrotech. 26 (4) (2001) 161–164.

[4] A. Hammerl, T.M. Klapötke, H. Nöth, M. Warchhold, $[N_2H_5]^+_2$ $[N_4C–N=N–CN_4]^{2-}$: a new high-nitrogen high-energetic material, Inorg. Chem. 40 (2001) 3570–3575.

[5] A. Hammerl, H. Gerhard, T.M. Klapötke, P. Mayer, H. Nöth, H. Piotrowski, M. Warchhold, Salts of 5,5′-azotetrazolate, Eur. J. Inorg. Chem. (2002) 834–845.

[6] S. Gurdip, P. Rishikesh, F. Roland, Studies on energetic compounds: part 45. Synthesis and crystal structure of disodium azotetrazole pentahydrate, J. Hazard. Mater. A 118 (2005) 75–78.

[7] G. Corsin, H. Keller Andreas, H. Konrad, Economic optimization of an industrial semibatch reactor applying dynamic programming, Ind. Eng. Chem. Res. 37 (1998) 4017.

[8] A.K. Gom Reddy, A. Chatterjee, Thermal study of the salts of azotetrazole, Thermochim. Acta 66 (1983) 231–244.

[9] G.M. Sheldrick, SHELXS-97, Program for X-ray Crystal Structure Determination, Göttingen University, Germany, 1997.

[10] G.M. Sheldrick, SHELXL-97, Program for X-ray Crystal Structure Refinement, Göttingen University, Germany, 1997.

[11] R.Z. Hu, Q.Z. Shi, Thermal Analysis Kinetics, Science Press, Beijing, 2001.